100 Gbps FlexE-over-DMT for B5G Optical Fronthaul using NLP-Optimized Preamble Equalization

Mohsan Niaz Chughtai[1], Shumaila Sabeen Gull[1], Minahil Qaisar[1]

[1]Department of Telecommunication Engineering, University of Engineering and Technology, Taxila, Pakistan.

*__Correspondence__: mohsan.niaz@uettaxila.edu.pk

Citation | Chughtai. M. N, Gull. S. S, Qasir. M, "100 Gbps FlexE-over-DMT for B5G Optical Fronthaul using NLP-Optimized Preamble Equalization", IJIST, Vol. 8 Issue. 5 pp 2311-2324, August 2026

DOI: https://doi.org/10.33411/IJIST/1985

Received | Aug 03, 2026 **Revised |** Aug 21, 2026 **Accepted |** Aug 22, 2026 **Published |** Aug 30, 2026.

FlexE is a key enabling technology for hardware-based isolation of different slices in 5G and beyond mobile networks, ensuring dedicated tunnels or 5 Gbps slots. This paper proposes an optimized DMT-based transport architecture for FlexE, achieving a 100 Gbps aggregate bitrate over 10 km of SSMF within the 3GPP EVM limits. Transporting 100 Gbps FlexE traffic over intensity-modulation direct-detection DMT links is limited by subcarrier and amplitude-dependent noise variance in high-order QAM constellations. To address this, a nonlinear programming-optimized weighted preamble equalization strategy is introduced to mitigate the imbalanced noise variance inherent in high-order QAM after zero-forcing equalization. Simulations for a system with 3800 active subcarriers, a 25-tap equalizer, and 4-, 16-, 64-, and 256-QAM modulation formats demonstrate that the proposed method reduces the required OSNR by 3.15 dB for 4-QAM at a 17.5% EVM threshold and 4.75 dB for 16-QAM at a 12.5% EVM threshold. For 64-QAM, the maximum measured OSNR improvement is 5.3 dB at 8 % EVM, while optimized preamble averaging provides an additional improvement of approximately 0.3 dB over conventional uniform preamble averaging. These results demonstrate that optimized preamble equalization improves the OSNR efficiency of DMT-based FlexE transport and its potential for power-efficient optical fronthaul.

Keywords: FlexE; DMT; Optimal Equalization; Noise Variance; 5G Fronthaul.

Introduction:

The evolution of advanced 5G to 6G networks has resulted in the development of different services such as holographic communications, digital twins, large-scale extended reality (XR), and AI-native services [1][2][3][4]. For the provisioning of these services, wider bandwidths, higher subcarrier spacings, massive MIMO scaling, and increasingly dynamic functional splits will be required in the network. The transport network links in the cross-haul (Xhaul) will require ultra-low deterministic latency, ultra-low jitter, and granular bandwidth provisioning [5][6]. Traditional Ethernet can be suitable for delivering such services; however, despite its ubiquity and cost efficiency, it struggles to provide deterministic scheduling and coarse bandwidth-rate granularity.

Recent work has further emphasized the importance of optical transport for 6G and disaggregated radio-access networks [6]. Optical fronthaul is being investigated because it can simultaneously support high capacity, low latency, synchronization, and flexible connectivity requirements in future radio-access architectures. Recent surveys identify elastic optical networking, passive optical networking, coherent and direct-detection transmission, photonic integration, and intelligent resource management as important technology directions for 6G fronthaul [7]. In parallel, recent studies have examined the capacity and latency requirements imposed by disaggregated 6G radio-access networks and have highlighted the need for transport architectures that combine scalable capacity with deterministic performance [8]. These requirements motivate the investigation of transport mechanisms that can provide both fine-grained bandwidth allocation and efficient physical-layer transmission.

Flexible Ethernet (FlexE) is particularly relevant, as it was introduced by the Optical Internetworking Forum (OIF) [9]. FlexE introduces a new layer called FlexE Shim in the transport layer of Ethernet between the media access layer (MAC) and the physical coding sublayer. The FlexE shim divides the incoming traffic into dedicated time slots of 5 Gbps, which can be allocated to different services or slices in 5G or future 6G networks [10]. These provisions the network operators to provide logical channels of 5 Gbps to dynamically varying fronthaul traffic with strict isolation and deterministic performance, which is the requirement for Radio-over-Ethernet (RoE), enhanced common public radio interface (eCPRI), and high-layer functional splits [11][12].

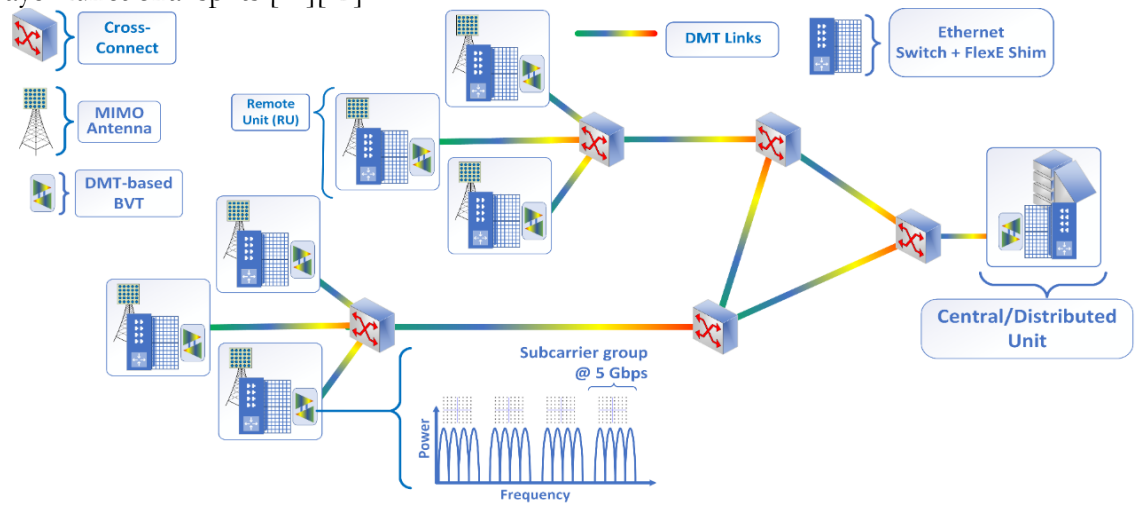


Figure 1. 5G and beyond fronthaul, with FlexE aggregation.

The research in the paper focuses on a digital fronthaul link where traffic is aggregated and disaggregated in the digital domain, which in this case can be done in the FlexE Shim or calendar. Traffic from different slices or functional splits in the 5G networks can be assigned a different number of FlexE slots in the form of groups to be transported over the Xhaul links. A conceptual representation of the 5G Xhaul and beyond is shown in Figure 1 [12][13].

In Figure 1, the remote units (RUs) and the central and distributed units (CU/DUs) are equipped with Ethernet switches equipped with FlexE shims or calendars. It is assumed in the analysis that Ethernet switches in RUs can aggregate traffic from different 5G network slices, such as Enhanced Mobile Broadband (eMBB), Ultra-Reliable Low-Latency Communications (uRLLC), and Massive Machine-Type Communications (mMTC), with different data rates. The traffic from these slices is then given a fixed number of 5 Gbps slots for hardware-level isolation, low latency, and high service reliability. The 5 Gbps slots from Flex Shims are transported over the physical channel using bandwidth-variable transponders (BVTs) based on discrete multitone modulation (DMT) transmission and reception. An example of the transmitted DMT multiplex signal transporting 5 Gbps slots is shown in the inset in Figure 1. It is assumed in Figure 1 that the cross-connects can also work as aggregation nodes equipped with BVTs and FlexE shims, and can direct the traffic to FlexE shims dedicated to different directions.

Earlier work established the suitability of FlexE for deterministic 5G fronthaul transport, while more recent research has considered FlexE over elastic optical networks, FlexE-based cost optimization, and resilient FlexE fronthaul design. These studies primarily address network dimensioning, survivability, or resource allocation [14][15]. They do not investigate the effect of amplitude-dependent post-equalization noise on FlexE traffic transported through a high-capacity IM/DD DMT physical link.

DMT-based FlexE transport in fronthaul:

Recently, intensity modulation direct detection (IMDD) and discrete multi-tone (DMT) based fronthaul links, such as (eCPRI), have been researched as a low-cost solution for 5G fronthaul network transport [16][17][18][19]. The key benefit is that for various Ethernet interface data rates, including 25 GbE, 50 GbE, 75 GbE, and 100 GbE, the subcarrier spacings, as well as the number of subcarriers, can be modified to accommodate the data rates within different bandwidths of the physical optical channel [17]. In addition to being a low-cost solution, a DMT system can mitigate the effects of frequency-selective channel impairments [20]. Fading at certain frequencies in fiber-optic communication can occur due to the linear and nonlinear impairments of the fiber optics, the nonlinear frequency responses of the modulator, laser source, and the photodetector [21].

To enable the transmission of fronthaul traffic using FlexE slots of 5 Gbps, multichannel DMT transmission has been demonstrated via simulations in [13], based on the simulation link parameters in [22]. DMT was demonstrated as it remains attractive for cost-sensitive optical fronthaul because it supports frequency-selective channel adaptation, flexible subcarrier loading, and direct detection.

The analysis does not elaborate on the performance of preamble averaging equalization in comparison to the conventional zero-forcing (ZF) equalization. The research in [23] and [24] established the basis for preamble-based synchronization; their methods focus on timing/frequency offset. Recent optical-DMT research has explored nonlinear and end-to-end equalization, adaptive Volterra processing, and joint optimization of transmitter and receiver parameters [25][26]. However, the research in the paper extends this concept by applying an ILP-based optimal weighting to preamble symbols, specifically to solve the post-equalization signal power-dependent noise variance in 100 Gbps FlexE-over-DMT fronthaul links.

Novelty and research objectives:

The novelties of the research in the paper are listed as follows:

- A 100-Gb/s FlexE-over-DMT IM/DD fronthaul architecture is evaluated using twenty 5-Gbps FlexE subcarrier groups over 10 km of standard single-mode fiber.

- The amplitude-dependent noise imbalance produced by zero-forcing equalization of high-order QAM symbols is identified and related to the received-symbol amplitude and channel-estimation variance.
- A constrained optimization problem is formulated to obtain the preamble-combining coefficients. The coefficients satisfy a unity-sum constraint and nonnegativity constraints, thereby preserving the scale of the channel estimate while preventing physically undesirable sign reversals.
- The method is compared with conventional pilot-based zero-forcing and uniform preamble averaging for QPSK/4-QAM, 16-QAM, 64-QAM, and 256-QAM.
- The results quantify the modulation-order dependence of the gain, showing that the advantage of weighted preamble equalization becomes more pronounced for higher-order QAM.

The research objectives of the paper are listed as follows:

- To design and simulate a 100-Gb/s FlexE-over-DMT IM/DD optical-fronthaul link consisting of twenty 5-Gb/s FlexE subcarrier groups.
- To characterize the performance of pilot-based zero-forcing equalization, uniform preamble averaging, and optimized weighted preamble averaging.
- To formulate a constrained optimization problem for determining the preamble-combining weights for each DMT subcarrier.
- To quantify the effect of the proposed equalizer on EVM and required OSNR for 4-QAM, 16-QAM, 64-QAM, and 256-QAM.
- To investigate how the number of equalizer taps affects the EVM and to select a tap count using a performance-complexity trade-off.
- To assess whether the proposed method provides statistically reliable performance improvements across repeated simulation realizations.

Preamble Averaging and Optimization Problem Formulation:

In ZF equalization, the estimated channel is given as follows [**Error! Reference source not found.**],

$$\hat{H}[k,n] = \frac{Y[k,n]}{X[k,n]} \tag{1}$$

where $X[k,n]$ is the transmitted pilot symbol for subcarrier, k and symbol index, n, $Y[k,n]$ is the received pilot symb

ol. After the estimation of the channel at the pilot indices, the overall channel response is estimated using nonlinear interpolation. Finally, the estimated transmitted sequence, $\hat{X}[k,n]$ is estimated by the following relation,

$$\hat{X}[k,n] = \frac{Y[k,n]}{H[k,n]} \tag{2}$$

where $H[k,n]$ is the overall estimated channel frequency response after interpolation of the pilot symbols' frequency response $\hat{H}[k,n]$.

However, ZF equalization enhances the noise in the received signal, and the variance of the noise also becomes dependent on the amplitude of the received signal symbol. The reason for this can be explained using the property for the variance of a number that is a product of a random variable and a constant [**Error! Reference source not found.**]. When used in the context of ZF channel equalization, the variance of the estimated symbol, $\hat{X}[k,n]$ in Equation (2), is given as follows,

$$Var\left(\hat{X}[k,n]\right) = \left(Y[k,n]\right)^2 Var\left(\frac{1}{H[k,n]}\right) \tag{3}$$

For a certain overall noise in the channel, the variance in the estimated channel, $H[k,n]$, gets 'amplified' by the power of the received QAM symbol, $Y[k,n]$, in Equation (3), resulting in a higher variance of the estimated QAM symbols, $\hat{X}[k,n]$. In other words, the QAM constellation points with higher amplitudes will have a larger noise variance after equalization in comparison to points with lower amplitudes, resulting in an imbalanced noise variance. The phenomenon will be shown in the results in Section 5.

It is assumed, for the research in the paper, that beyond 5G fronthaul networks will use digital fronthaul, where aggregation and de-aggregation of data streams from different splits/layers are carried out in the digital domain. This converts the overall channel for the DMT system into a time-invariant or constant, eliminating the need to constantly transmit the pilot symbols and motivating the use of preamble-based equalization. To overcome the imbalanced noise variance in the equalized QAM constellation, the research in the paper utilizes optimal weighted preamble-averaging-equalization instead of pilot-based equalization. In this method, the preamble/reference DMT symbols are sent over all the subcarriers and a minor portion of the total number of transmitted DMT symbols. The preamble symbols comprise independent and uniformly distributed QAM symbols with the same modulation level being used for data transmission. At the receiver, the channel is estimated for every symbol in the preamble, and the overall channel is estimated by calculating the average of the channel estimates along the time axis [**Error! Reference source not found.**]. The estimated channel response for preamble-averaging-based equalization is given as follows,

$$\bar{H}[k] = \frac{1}{N}\sum_{n=1}^{N_p} \hat{H}[k,n] \tag{4}$$

where $\bar{H}[k]$, is the averaged estimate of the channel over N_p DMT preamble symbols for the subcarrier k and, $\hat{H}[k,n]$ is the channel estimate, using Equation (1), at the subcarrier k and n^{th} DMT symbol.

Preamble-averaging in Equation (4) removes the post-equalization imbalanced noise variance dependent on QAM symbol amplitudes. It does so by averaging the noise in the channel estimate, $H[k,n]$ in Equation (1), and reducing the variance, $Var(1/H[k,n])$ in Equation (3), thus significantly improving the error vector magnitude (EVM).

Further improvements in the performance can also be achieved by calculating the coefficients of the averaging filter such that the error between the transmitted preamble symbols and received symbols is minimized for every sub-carrier in the DMT symbol. In this research, the weights of the optimal averaging filter were calculated using an optimization problem given as follows,

$$\bar{H}[k] = \sum_{n=1}^{N_p} w[k,n]\hat{H}[k,n] \tag{5}$$

where, $w[k,n]$, are the weights of the averaging filter that minimize the mean square error between the transmitted preamble symbols, N_p, and equalized symbols for a subcarrier index, k and n^{th} DMT symbol. For calculating the optimal filter coefficient vector, $w_k = \left[w[k,1], \ldots., w[k,N_p]\right]^T$, the mean square error minimization problem is given as follows,

$$\min_{w_k} J_k(w_k) = \sum_{n=1}^{N_p} \left| P[k,n] - \frac{Y[k,n]}{\bar{H}[k]} \right|^2 \tag{6}$$

where J_k is the subcarrier-specific preamble mean-square error, $P[k,n]$, are the preamble symbols for a subcarrier k and n^{th} DMT symbol, $\bar{H}[k]$ is the channel estimate for

the subcarrier, k, calculated using Equation (5). The error in Equation (6) is minimized subject to the following constraints,

$$\sum_{n=1}^{N_p} w[k,n] = 1 \tag{7}$$

and,

$$0 \le w[k,n] \le 1, \quad n = 1, \ldots\ldots, N_p \tag{8}$$

The unity-sum constraint in Equation (7) prevents a gain bias in the combined channel estimate, while the nonnegativity constraint in Equation (8) ensures that the estimator forms a convex combination of the available channel estimates.

Note that the nonlinear programming (NLP) problem is solved using Sequential Quadratic Programming (SQP) initialized with uniform weights. $w_0 = \left[1/N_p, \ldots\ldots, 1/N_p\right]^T$ in MATLAB® using the 'fmincon' function. The SQP solver is configured with strict termination criteria, including a first-order optimality tolerance of 10^{-6}, a minimum step size tolerance of 10^{-6}, and a maximum limit of 400 iterations to guarantee convergence while enforcing the probability simplex constraints in Equation (7) and Equation (8).

The proposed weighted preamble equalizer has higher channel-estimation complexity than conventional zero-forcing (ZF) equalization. ZF requires approximately $O(K)$ operations for K active subcarriers, whereas the proposed method requires $O(KT)$ operations to combine T preamble observations, in addition to the constrained NLP-solver cost C_{NLP}. However, the optimization is performed only during preamble-based channel estimation; subsequent data equalization remains. $O(K)$, as in ZF. With $T = 25$ taps, the method provides a practical performance-complexity trade-off, incurring additional initialization or channel-tracking overhead in exchange for the reported OSNR improvement. The computational techniques compared in the paper are also summarized in Table 1.

Table 1. Computational complexity comparison of equalization techniques.

Equalization method	Channel-estimation operations per subcarrier	Data equalization per symbol	Approximate complexity
Conventional ZF	One channel estimate	One complex division	$O(K)$
Uniform preamble averaging	T channel estimates and T additions	Uniform preamble averaging	$O(KT)$
Proposed weighted preamble equalization	Proposed weighted preamble equalization T, channel estimates, weighted products T, and NLP optimization	One complex division	$O(KT) + C_{NLP}$

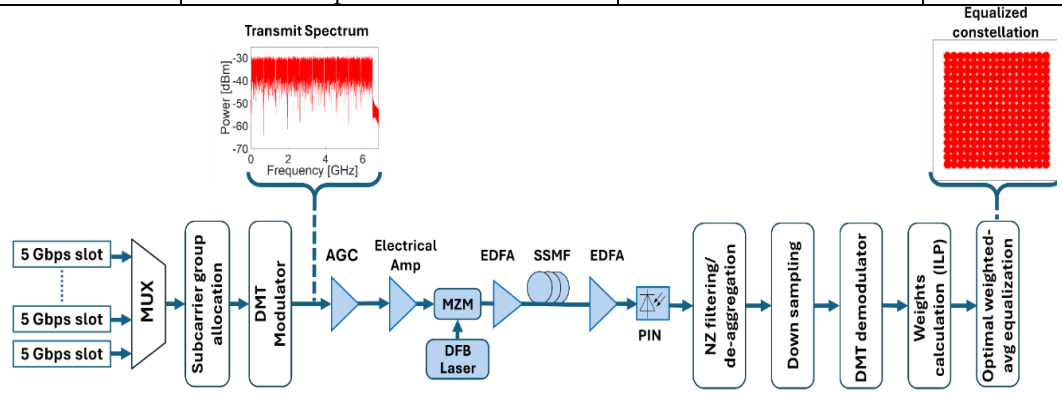


Figure 2. Simulation setup of the DMT link.

The proposed weighted preamble equalizer is suitable for FPGA/ASIC implementation because the optimization is performed only during preamble-based channel estimation. After the weights are obtained, data symbols use the same one-tap complex equalization operation as conventional ZF. The receiver can be divided into FFT demodulation, channel estimation, weight optimization, and data equalization.

The constrained nonlinear-programming operation is less suitable for execution at the full symbol rate because it requires iterative updates and repeated evaluations of the objective function. In a practical transceiver, the optimization can therefore be implemented in one of three ways: (i) executed by an embedded processor during initialization, (ii) executed periodically by a background control processor for slow channel tracking, or (iii) replaced by a hardware-oriented approximation using a fixed iteration count, a lookup table, or precomputed coefficient sets. Since the proposed link is assumed to be time-invariant over the preamble/data interval, the optimized coefficients need not be recalculated for every data symbol.

The present study is simulation-based and does not include FPGA resource utilization, fixed-point analysis, power consumption, or processing latency; these aspects will be investigated through future hardware-in-the-loop or FPGA-prototype validation.

Simulation Setup for DMT-based FlexE transport:

The DMT-based fronthaul link to transmit FlexE slots of 5 Gbps was tested using simulations in Optisystem® ver. 14 and is given in Figure 2. It represents an end-to-end link between an RU and a CU/DU, or between an RU and an aggregation node equipped with a FlexE shim in Figure 1.

Within the DMT modulator block in Figure 2, the data for simulations is generated in the form of uniformly distributed quadrature amplitude modulation (64-QAM) symbols for each slot of 5 Gbps, which is termed a 'subcarrier group'. The simulation parameters used in the paper were the same as those used for research in [13], [22]. The system parameters for the 100 Gbps DMT optical transmission setup were selected to align with the stringent performance requirements of B5G/6G C-RAN fronthaul networks. A 10 km Standard Single-Mode Fiber (SSMF) link was adopted in accordance with 3GPP TS 38.801 and O-RAN Alliance specifications for Category B short-reach fronthaul connections between the Distributed Unit (DU) and Radio Unit (RU) [29].

The Discrete Multi-Tone (DMT) grid uses a subcarrier spacing (SCS) of 220 kHz, yielding a short symbol duration ($T_{sym} \approx 4.55\ \mu s$) that minimizes transmission latency while providing robust resilience against laser linewidth phase noise [30]. Therefore, 3800 subcarriers with an SCS of 220 kHz were selected to match the nominal 5 Gbps FlexE slot rate for the reference 64-QAM configuration. In total, 20 groups of 3800 subcarriers were transmitted over the fiber optic channel, making the aggregate data rate 100 Gbps. Results were collected using QPSK, 16QAM, 64QAM, and 256QAM modulation of subcarrier groups.

To accommodate physical hardware constraints, a 24 MHz guard band is incorporated between the subcarrier group edges; this suppresses out-of-band emissions, isolates carrier leakage and flicker noise, and provides a gradual transition region for DAC/ADC anti-aliasing filter roll-off. The cyclic prefix is set to 12.5% of the DMT symbol duration to absorb the effective channel-memory spread produced by the simulated electrical and optical link.

The overall sampling frequency of the simulation setup was 17.22 GHz, as a product of the total number of points in the IFFT operation, to convert the frequency-domain signal to the time domain at the transmitter in the DMT modulator in Figure 2, and spacing of 220 KHz of each subcarrier.

The transmitter in Figure 2 comprises a laser source operating at a frequency of 193.1 THz and a linewidth of 0.1 MHz. The Mach-Zehnder modulator (MZM) in Figure 2 had a 4V as the V_π, and 2V as the biased operating point. Note that the MZM was biased at 2V to ensure

that the peak-to-peak swing of the DMT multiplex signal is less than 2V and results in the least back-to-back error vector magnitude (EVM).

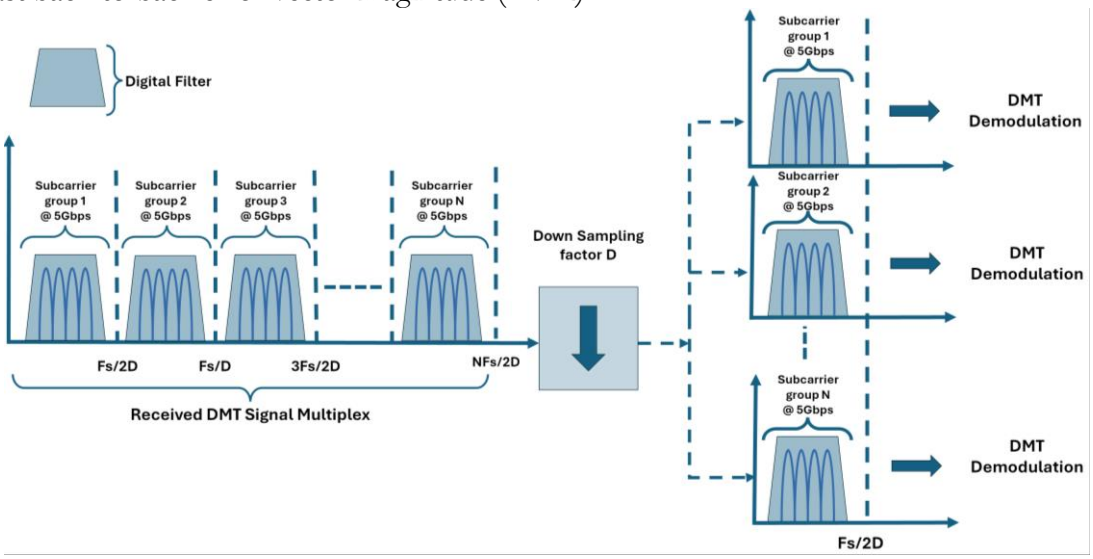


Figure 3. Digital down-conversion of the received DMT multiplex signal.

The DMT multiplex signal was used as the input drive signal to the MZM to modulate the optical carrier from the laser source. An optical erbium-doped fiber amplifier (EDFA) in Figure 2, with a gain of 6 dB and a 4 dB noise figure (NF), was used as an optical pre-amplifier. The amplified signal propagates through a standard single-mode fiber (SSMF) in Figure 2 with a length of 10 km, a loss of 0.2 dB/km, a chromatic dispersion parameter of 16.75 ps/nm/km, and a Kerr coefficient n_2, of 26×10^{-21} m^2/W and an effective area, A_{eff}, of 80 μm^2. After transmission, the signal is pre-amplified by an EDFA with a gain of 2 dB and a noise figure of 4 dB. The signal was detected by a positive-intrinsic-negative (PIN) photodetector, in Figure 2, with a responsivity of 1 A/W. and a thermal noise density of 15×10^{-24} W/Hz.

After photodetection, the received DMT multiplex signal was sampled via the Nyquist zone de-mapping in MATLAB®, demonstrated previously in [31] and shown in Figure 3. In the received DMT multiplex signal, the received subcarrier groups of 5 Gbps are digitally filtered separately, are shown in blue in Figure 3 and are then down-sampled by a factor of D, being the ratio of the overall sampling rate and per-channel sampling rate. This results in each subcarrier group representing a Nyquist zone that folds back to intermediate frequency (IF). Each subcarrier group is then demodulated separately via DMT demodulation. The DMT demodulation process involves removal of the cyclic prefix, the FFT operation, removal of Hermitian symmetry, equalization, and estimation of transmitted symbols.

Finally, an equalizer length of 25 filter taps was chosen based on empirical EVM convergence sweeps (Figure 6), fully compensating for chromatic dispersion-induced inter-symbol interference (D≈16.75 ps/nm/km) without introducing unnecessary DSP computational complexity.

It is clarified that the study is based on simulations, so it assumes ideal synchronization, a fixed 10-km fiber span, and time-invariant channel and component responses; therefore, timing errors, phase noise, drift, aging, and changing noise conditions are not considered. Finally, the simulation-based results do not account for finite-precision effects, hardware latency, resource utilization, or experimental constraints. Future work will investigate adaptive synchronization and channel tracking, different transmission distances, parameter optimization, and FPGA/ASIC validation.

Results for DMT-based FlexE transport:

To assess the performance of the zero forcing, preamble averaging, and optimal preamble averaging equalization techniques, Initially, simulations of the link in Figure 2 were carried out at 100 Gbps using 64 QAM modulation, with a total DMT-multiplex bandwidth of 17.22 GHz. The results were collected by transmitting a total of 3.8×10^6 QAM symbols (3,800 subcarriers × 20 DMT frames × 50 channel/noise realizations). The performance of the equalization techniques was evaluated using error vector magnitudes (EVMs) for the QAM symbols after the equalization of the received DMT signal frames. The performance of the equalization techniques for different modulation formats was compared in terms of optical signal-to-noise ratio (OSNR) gains at the standard 3GPP EVMs.

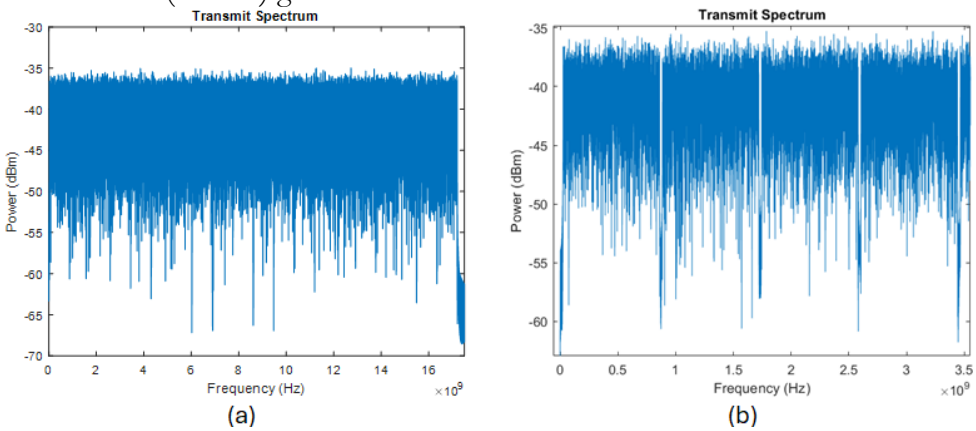


Figure 4. Transmit spectrum of DMT signal at 100 Gbps using 64 QAM (a), transmit spectrum for 4 out of 20, 5 Gbps slots (b).

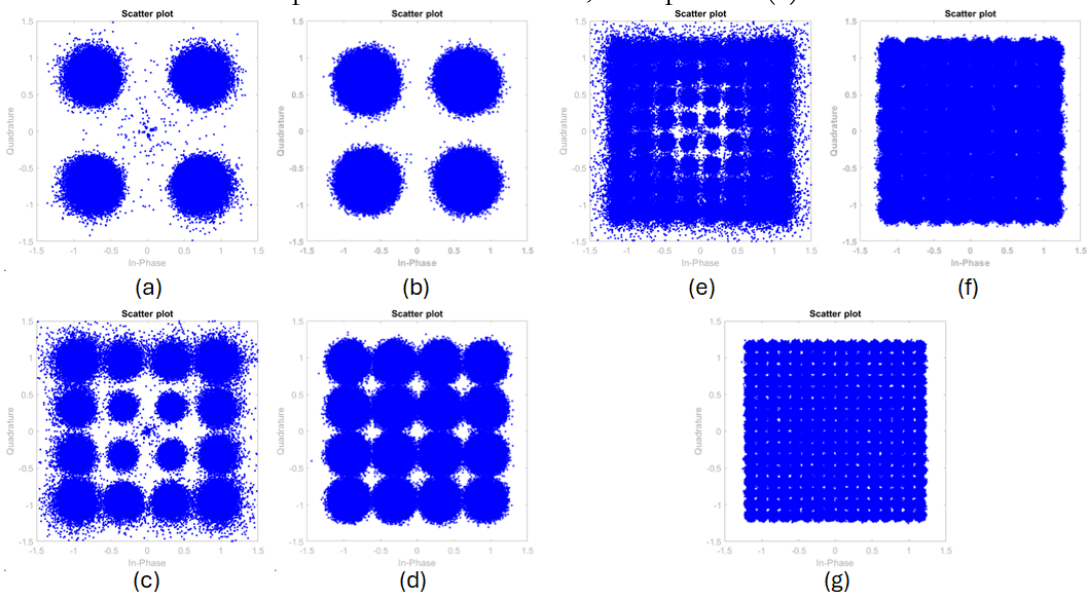


Figure 5. Equalized constellation using pilot-based equalization (a), (c), (e), and preamble-averaging-based equalization (b), (d), (f), (g) for 4 QAM, 16 QAM, 64 QAM, 256 QAM, and 17.5%, 12.5%, 8%, and 3.5% EVMs.

The performance was assessed by sweeping the transmit power of the laser source from 10 dBm to 25 dBm. Assuming the system is dominated by amplified spontaneous noise (ASE) added by the EDFAs and considering the power loss due to the power transmission function of the MZM modulator, as well as the attenuation in the fiber optic channel, the power sweep resulted in an OSNR sweep from 58.22 dB to 73.22 dB. Note that the OSNR was calculated as a ratio of the measured transmitted optical power at the output of the MZM, in Figure 2, and the ASE noise from two EDFAs, in Figure 2, calculated over the entire

bandwidth of the DMT multiplex. The transmitted signal spectrum for 100 Gbps using 64 QAM modulation is shown in Figure 4.

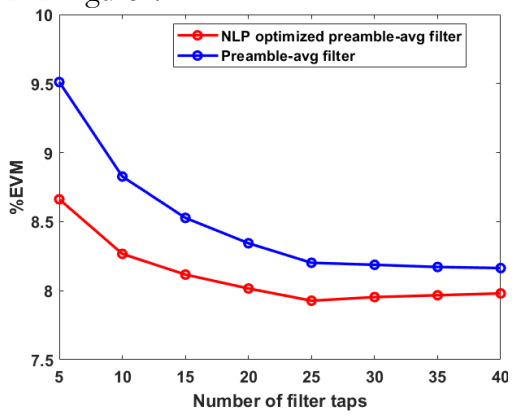


Figure 6. EVM vs number of filter taps for preamble-averaging-based equalization.

As an example, for the performance of preamble averaging equalization in comparison to pilot-based ZF equalization, the equalized constellation diagrams are shown side by side in Figure 5, at standard EVMs of 17.5 %, 12.5 %, 8%, and 3.5% using 4 QAM, 16 QAM, 64 QAM, and 256 QAM, respectively. From the analysis in Figure 5 (a), (c), (e), it can be observed that in the cases of pilot-based equalization, the equalized constellation has an imbalanced variance of noise that is dependent on the constellation amplitudes, as discussed in Equation (3). The preamble-averaging equalization solves this problem, and the equalized constellations in Figure 5 (b), (d), (f), (g) have balanced noise variances, thus resulting in less required launched powers to achieve the same EVM performance.

The performance of equalization using preamble-averaging and optimal-preamble averaging for Equation (5), for the same DMT system operating at 100 Gbps, using 64 QAM, at a launch power of 12 dBm, with an increasing number of taps from 5 to 40 taps, is shown in Figure 6. From the analysis of Figure 6, it is concluded that the EVM reduces with the increasing number of taps for both preamble averaging and optimal averaging equalization. This trend occurs because a higher tap count provides the filter with more degrees of freedom to resolve the channel's frequency response.

Beyond 25 taps, there is no significant gain in performance in terms of reduction of EVM. The performance gain from optimal preamble averaging is higher for fewer taps and decreases as the number of taps increases. This is attributed to the NLP solver's ability to find a globally optimized weight vector that compensates for residual noise with fewer filter lengths, whereas at higher tap counts, the increased resolution of the standard method allows it to converge toward the same performance. The highest gain in EVM performance in Figure 6 is 0.8% for 5 taps and reduces to a minimum of 0.2% for 40 taps. The lowest EVM is achieved with 25 taps at 7.9%. Therefore, 25 taps were used in the research for both preamble-averaging and optimal averaging equalization.

The EVM results for the transmission of 100 Gbps using 64 QAM, using pilot-based equalization in Equation (2), preamble-averaging-based equalization in Equation (4), and optimal averaging in Equation (5) are given in the following Figure 7. From the analysis of Figure 7, it is concluded that the preamble-averaging-based equalization performs better than the pilot-based equalization. Specifically, for a threshold of 8% EVM standard of 3GPP [32], pilot-based equalization requires approximately 5 dB higher OSNR.

Optimal averaging-based equalization performs better than preamble-averaging equalization by 0.3 dB; thus, the best overall gain in performance was 5.3 dB. The narrow 0.3 dB performance gap indicates that the system is operating in a noise-limited regime. Because the 10 km link and the cyclic prefix effectively mitigate signal distortion, equalization

performance is constrained by the signal-to-noise ratio (SNR) floor of the system rather than residual interference. Consequently, standard preamble averaging already performs near the physical limit, leaving little room for further gain through NLP-based optimization.

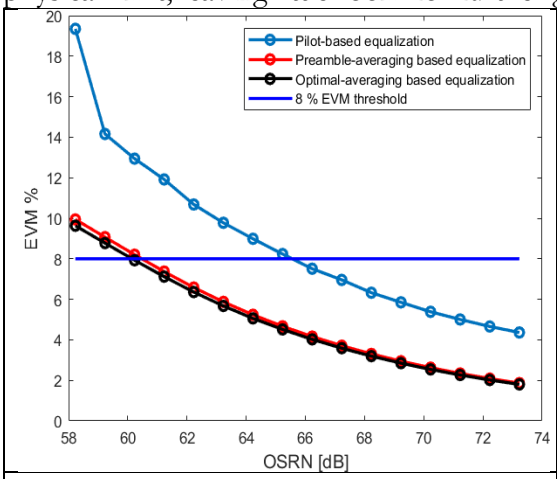


Figure 7. EVM vs OSNR at 100 Gbps and 64 QAM

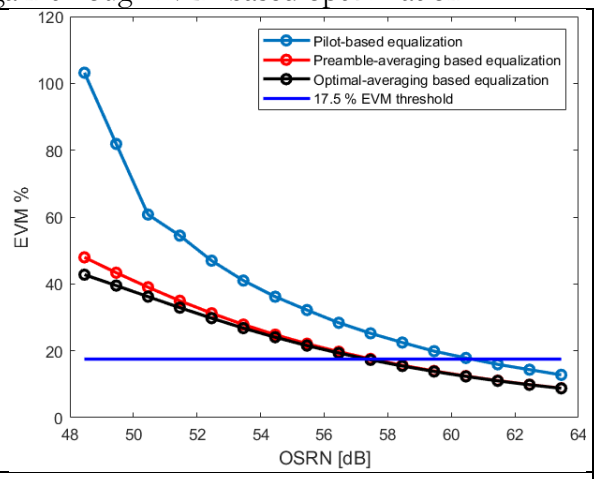


Figure 8. EVM vs OSNR for 100 Gbps and 4 QAM

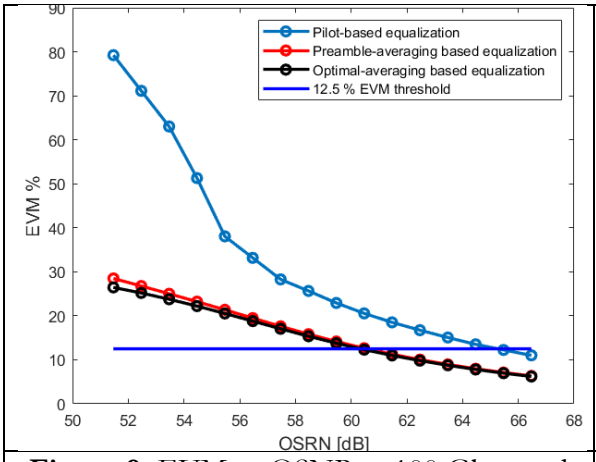


Figure 9. EVM vs OSNR at 100 Gbps and 16 QAM.

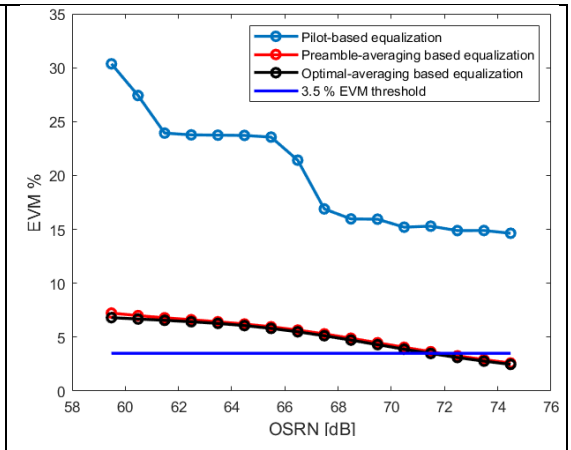


Figure 10. EVM vs OSNR at 100 Gbps and 256 QAM.

Given the large statistical sample size, the margin of error for the measured EVM near the convergence threshold of 7.9% is within ±0.12%. Correspondingly, the reported 5.3 dB OSNR demand for the NLP-weighted scheme exhibits a tight confidence bound of 5.3 ± 0.08 dB, compared to 10.6 ± 0.11 dB for conventional Zero-Forcing equalization. The clear separation between these confidence bounds confirms that the observed 5.3 dB OSNR improvement is statistically significant and robust against random noise variations.

To assess the performance of equalization based on optimal weighted preamble averaging in comparison to pilot-based ZF equalization, the transmission of FlexE slots was also tested using 4QAM, 16QAM, and 256QAM modulation formats in DMT. The number of subcarriers for a subcarrier group was fixed at 3800 for all modulation formats. The electrical transmit powers of the DMT signal for the three cases (4 QAM, 16 QAM, and 256 QAM) were normalized to the transmit power for the 64 QAM modulation case, for a fair comparison. The laser source optical launch power was varied between 5–20 dBm (4-QAM, 16-QAM) and 10–25 dBm (64-QAM, 256-QAM). The EVMs vs the OSNRs for the 4-QAM, 16-QAM, and 256-QAM transmissions are given in Figure 8-10. The gain in performance in terms of OSNR is 3.15 dB for 4-QAM transmission for an EVM threshold of 17.5% in Figure

8; it is 4.75 dB for 16-QAM transmission for an EVM threshold of 12.5% in Figure 9, and the performance of ZF equalization was not able to achieve the EVM of 3.5% for 256-QAM in Figure 10. The results for OSNR gains are also compiled in the following Table 2.

It can be concluded from the results in Figures 7–10 that, as the modulation level increases, the OSNR gain also increases for optimal preamble-averaging equalization compared to ZF equalization. The OSNR gain increases as higher-order QAM formats are more sensitive to post-equalization noise imbalance, as shown in Figure 5 and channel estimation errors. Optimal weighted preamble-averaging equalization mitigates this issue, so its relative advantage over ZF increases as the modulation order increases.

Table 2. OSNR gains for different equalization techniques and modulation formats.

Modulation Format	EVM Threshold (%)	Pilot-Based Equalization (OSNR)	Preamble-Avg Based Equalization (OSNR)	Optimal-Avg Based Equalization (OSNR)	OSNR Gain (Proposed vs. Pilot-Based)
4-QAM	17.5%	60.8 dB	57.8 dB	57.65 dB	3.15 dB
16-QAM	12.5%	65.2 dB	60.6 dB	60.45 dB	4.75 dB
64-QAM	8.0%	65.63 dB	60.63 dB	60.33 dB	5.3 dB
256-QAM	3.5%	Unachievable	71.8 dB	71.40 dB	

Conclusion:

The research in the paper demonstrates the feasibility of DMT-based optical transmission for Flexible Ethernet, demonstrating the potential for an efficient and scalable solution for beyond 5G fronthaul transport. By leveraging the adaptability of DMT and the granularity of FlexE technology, the research addresses the granular, high-capacity requirements for future fronthaul networks while maintaining robustness against channel impairments.

A detailed system analysis was conducted for a short 10 km fiber optic DMT-based transmission link using an external laser source and Mach-Zehnder modulator. The research focused on DMT signal processing, where the optimal weighted preamble-averaging equalization technique was introduced to improve the system performance in comparison to conventional pilot-based zero-forcing equalization. The results confirm that optimal averaging provides measurable gains in OSNR performance, thereby demonstrating the potential for improved transmission reach and capacity. From a networking perspective, FlexE enabled by DMT and preamble-averaging-based equalization presents a promising solution for dynamic optical bandwidth allocation to heterogeneous fronthaul traffic.

Despite the promising results, the study was limited to simulation-based analysis. Future work can incorporate experiment-based analysis, where temperature-based bias drift and long-term linear and nonlinear impairment evolution can also be included for longer reach distances. Furthermore, adaptive bit loadings and power allocation strategies can also improve the system-level performance.

Recently, several techniques for equalization using deep learning (DL), such as convolutional neural networks (CNNs), have been used for equalization in OFDM-based fiber optic transmission systems; their integration introduces substantial offline training overhead and high inference complexity during online payload processing. Exploring DL-assisted adaptive equalization as a trade-off between model complexity and performance remains a prospective topic for future extension of this work.

Conflict of interest: The authors declare that there is no conflict of interest regarding the publication of this manuscript in the International Journal of Indigenous Science and Technology (IJIST).

Project details: No funding was received.

References:

[1] D. H. Tran *et al.*, "Network Digital Twin for 6G and Beyond: An End-to-End View Across Multi-Domain Network Ecosystems," *IEEE Open J. Commun. Soc.*, vol. 6, pp. 6866–6911, 2025, doi: 10.1109/OJCOMS.2025.3599866.

[2] "Samsung Electronics Unveils 6G White Paper and Outlines Direction for AI-Native and Sustainable Communication – Samsung Global Newsroom." Accessed: Aug. 03, 2026. [Online]. Available: https://news.samsung.com/global/samsung-electronics-unveils-6g-white-paper-and-outlines-direction-for-ai-native-and-sustainable-communication

[3] Mika Ylianttila, Raimo Kantola, Andrei Gurtov, "6G White paper: Research challenges for Trust, Security and Privacy," *arXiv:2004.11665*, 2020, [Online]. Available: https://arxiv.org/abs/2004.11665

[4] T. Nakamura, "5G Evolution and 6G," *Dig. Tech. Pap. - Symp. VLSI Technol.*, vol. 2020-June, Jun. 2020, doi: 10.1109/VLSITECHNOLOGY18217.2020.9265094.

[5] D. Breskovic, "X-haul solutions for 5G/6G networks: Overview of requirements and technologies," *Comput. Networks*, vol. 274, p. 111796, Jan. 2026, doi: 10.1016/J.COMNET.2025.111796.

[6] A. Fayad, T. Cinkler, and J. Rak, "Toward 6G Optical Fronthaul: A Survey on Enabling Technologies and Research Perspectives," *IEEE Commun. Surv. Tutorials*, vol. 27, no. 1, pp. 629–666, 2025, doi: 10.1109/COMST.2024.3408090.

[7] G. Evsukoff, Y. Shang, E. A. Hoyos, H. Fabio Bermúdez-Orozco, J. A. Aldana-Gutierrez, and J. A. A. Co, "Towards 6G: A Review of Optical Transport Challenges for Intelligent and Autonomous Communications," *Comput. 2025, Vol. 13, Page 286*, vol. 13, no. 12, p. 286, Dec. 2025, doi: 10.3390/COMPUTATION13120286.

[8] A. Larranaga *et al.*, "Fronthaul/Midhaul Networks: Capacity and Latency Requirements Imposed by 6G Disaggregated RANs," *IEEE Commun. Mag.*, vol. 63, no. 5, pp. 86–93, 2025, doi: 10.1109/MCOM.002.2400419.

[9] "Implementation Agreements – OIF." Accessed: Aug. 03, 2026. [Online]. Available: https://www.oiforum.com/technical-work/implementation-agreements-ias/

[10] "What Is FlexE? What Are the Application Scenarios of FlexE? - Huawei." Accessed: Aug. 03, 2026. [Online]. Available: https://info.support.huawei.com/info-finder/encyclopedia/en/FlexE.html

[11] "Universal aggregation for service providers - Ciena." Accessed: Aug. 03, 2026. [Online]. Available: https://www.ciena.com/insights/articles/universal-aggregation-for-service-providers.html

[12] D. Koulougli, K. K. Nguyen, and M. Cheriet, "eCPRI Supports In 5G O-RAN Fronthaul With FlexEthernet," *Proc. - IEEE Glob. Commun. Conf. GLOBECOM*, pp. 1968–1973, 2023, doi: 10.1109/GLOBECOM54140.2023.10436913.

[13] M. N. Chughtai, P. Assimakopoulos, and N. J. Gomes, "Reinforcement Learning-Assisted Transmit Signal Power Savings in Variable Bit-Rate Fronthaul," *IEEE Commun. Lett.*, vol. 28, no. 6, pp. 1313–1316, Jun. 2024, doi: 10.1109/LCOMM.2024.3386848.

[14] D. Koulougli, K. K. Nguyen, and M. Cheriet, "Cost Optimization of FlexEthernet Over Elastic Optical Network Fronthaul Design," *IEEE Trans. Netw. Serv. Manag.*, vol. 22, no. 4, pp. 3120–3137, 2025, doi: 10.1109/TNSM.2025.3553417.

[15] D. Koulougli and K. K. Nguyen, "High-Resilient FlexEthernet over Elastic Optical Networks for Open RAN Backup Fronthaul Design," *Proc. - IEEE Glob. Commun. Conf. GLOBECOM*, pp. 3115–3120, 2025, doi: 10.1109/GLOBECOM59602.2025.11432336.

[16] S. C. J. Lee, "Discrete multitone modulation for short-range optical communications," 2009, doi: 10.6100/IR656509.

[17] S. T. Le *et al.*, "100Gbps DMT ASIC for Hybrid LTE-5G Mobile Fronthaul Networks," *J. Light. Technol.*, vol. 39, no. 3, pp. 801–812, Feb. 2021, doi: 10.1109/JLT.2020.3044516.

[18] S. T. Le, T. Drenski, A. Hills, M. King, and T. Sizer, "High-speed real-time transmissions supporting LTE/5G mobile fronthaul networks using discrete multitone format," *https://doi.org/10.1117/12.2577892*, vol. 11713, p. 53, Mar. 2021, doi:

10.1117/12.2577892.
[19] "IM/DD transmission techniques for emerging 5G fronthaul, DCI and metro applications | IEEE Conference Publication | IEEE Xplore." Accessed: Aug. 03, 2026. [Online]. Available: https://ieeexplore.ieee.org/document/7937039
[20] F. Cruz-Roldan, W. A. Martins, P. S. R. Diniz, and M. Moonen, "Achievable Data Rate of DCT-Based Multicarrier Modulation Systems," *IEEE Trans. Wirel. Commun.*, vol. 18, no. 3, pp. 1739–1749, Mar. 2019, doi: 10.1109/TWC.2019.2896073.
[21] K. Zhang, Q. Zhuge, H. Xin, W. Hu, and D. V. Plant, "Performance comparison of DML, EML and MZM in dispersion-unmanaged short reach transmissions with digital signal processing," *Opt. Express, Vol. 26, Issue 26, pp. 34288-34304*, vol. 26, no. 26, pp. 34288–34304, Dec. 2018, doi: 10.1364/OE.26.034288.
[22] S. Noor, P. Assimakopoulos, and N. J. Gomes, "A Flexible Subcarrier Multiplexing System with Analog Transport and Digital Processing for 5G (and Beyond) Fronthaul," *J. Light. Technol.*, vol. 37, no. 14, pp. 3689–3700, Jul. 2019, doi: 10.1109/JLT.2019.2918215.
[23] P. H. Moose, "A Technique for Orthogonal Frequency Division Multiplexing Frequency Offset Correction," *IEEE Trans. Commun.*, vol. 42, no. 10, pp. 2908–2914, 1994, doi: 10.1109/26.328961.
[24] T. M. Schmidl and D. C. Cox, "Robust frequency and timing synchronization for OFDM," *IEEE Trans. Commun.*, vol. 45, no. 12, pp. 1613–1621, 1997, doi: 10.1109/26.650240.
[25] V. Q. Phuoc *et al.*, "An optimized LSTM-based equalizer for 100 Gigabit/s-class short-range fiber-optic communications," *AIMS Electron. Electr. Eng.*, vol. 8, no. 4, pp. 404–419, Nov. 2024, doi: 10.3934/ELECTRENG.2024019.
[26] S. Hernandez, C. Peucheret, F. Da Ros, and D. Zibar, "End-to-end optimization of optical communication systems based on directly modulated lasers," *J. Opt. Commun. Netw.*, vol. 16, no. 8, pp. D29–D43, Aug. 2024, doi: 10.1364/JOCN.522761.
[27] Y. S. Cho, J. Kim, W. Y. Yang, and C. G. Kang, "Mimo-Ofdm Wireless Communications With Matlab®," *MIMO-OFDM Wirel. Commun. With Matlab*, pp. 1–439, Jan. 2010, doi: 10.1002/9780470825631.
[28] "All of Statistics: A Concise Course in Statistical Inference | Springer Nature Link." Accessed: Aug. 24, 2026. [Online]. Available: https://link.springer.com/book/10.1007/978-0-387-21736-9
[29] "Transport network support of IMT-2020/5G - ITU." Accessed: Aug. 24, 2026. [Online]. Available: https://www.itu.int/hub/publication/t-tut-home-2018/
[30] D. T. Pham, M. K. Hong, J. M. Joo, E. S. Nam, and S. K. Han, "Laser phase noise and OFDM symbol duration effects on the performance of direct-detection based optical OFDM access network," *Opt. Fiber Technol.*, vol. 17, no. 3, pp. 252–257, May 2011, doi: 10.1016/J.YOFTE.2011.02.011.
[31] "Experimental demonstration of sub-Nyquist sampling for bandwidth- and hardware-efficient mobile fronthaul supporting 128×128 MIMO with 100-MHz OFDM signals | IEEE Conference Publication | IEEE Xplore." Accessed: Aug. 03, 2026. [Online]. Available: https://ieeexplore.ieee.org/document/7537756
[32] "3GPP (2018) 3GPP TS 38.104 Version 15.2.0 Release 15. 5G; NR; Base Station (BS) Radio Transmission and Reception. - References - Scientific Research Publishing." Accessed: Aug. 03, 2026. [Online]. Available: https://www.scirp.org/reference/referencespapers?referenceid=2859698



Copyright © by authors and 50Sea. This work is licensed under Creative Commons Attribution 4.0 International License.